Sequentially Controlled Dynamic Deployment of Ultra-Thin Shell Structures

Antonio Pedivellano*, Eleftherios E. Gdoutos †, and Sergio Pellegrino‡
California Institute of Technology, Pasadena, CA, 91125

This paper presents an approach to achieve the staged deployment of planar structures composed of multiple thin-shell elements. Releasable constraints are used to prescribe intermediate, known configurations along a strain energy-driven deployment path. An analytical model is derived to design the nominal deployment sequence of the structure by identifying kinematically compatible paths. Then, a finite element model is developed to capture the dynamic behavior of the shells during a staged deployment. Practical considerations, such as the deployment envelope and incorporation of the structure in a deployment mechanism are discussed. Finally, the proposed deployment sequence is demonstrated experimentally.

I. Introduction

Recently proposed spacecraft architectures envisage large two-dimensional apertures based on ultra-thin shell components. Commonly used for deployable booms, ultra-thin shell structures combine high deployed stiffness with compact packaging, which is achieved either by coiling [1][2] or folding [3]. The one-dimensional packaging schemes used for booms are not compatible with planar structures, for which a combination of folding and coiling techniques is required. From the deployment perspective, folded shells are generally deployed by releasing the constraints applied during packaging and letting the structure self-deploy using its stored elastic energy.

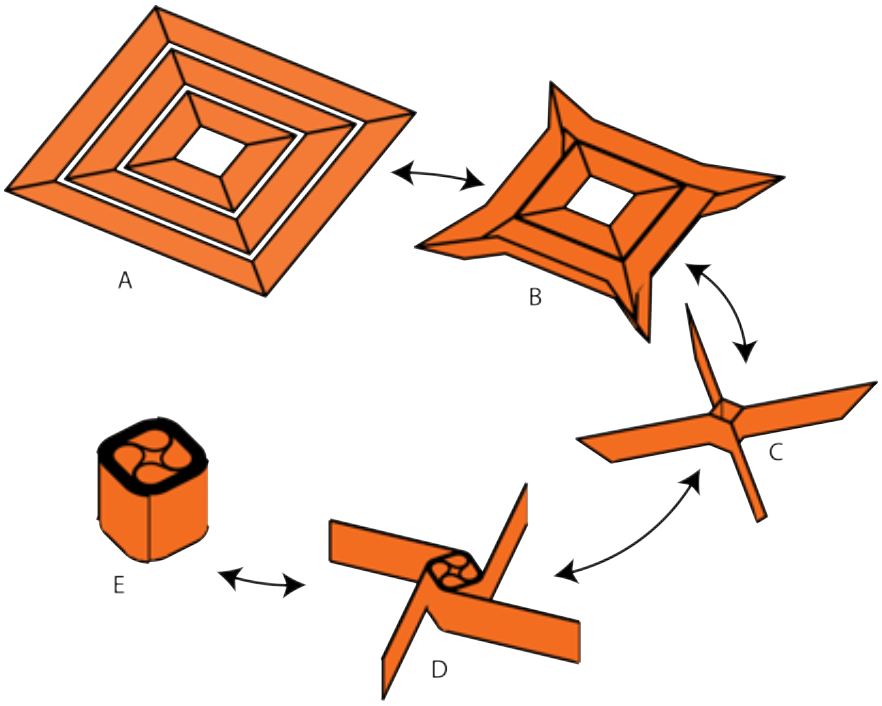

Fig. 1 Two-dimensional packaging scheme for a square space structure: folding (A to C) and coiling (C to E)

*Graduate student, Graduate Aerospace Laboratories, 1200 E.California Blvd Pasadena. E-mail: apedivel@caltech.edu
†Research Scientist, Graduate Aerospace Laboratories, MC 105-50. AIAA Member. E-mail: egdoutos@caltech.edu
‡Joyce and Kent Kresa Professor of Aerospace and Civil Engineering, Graduate Aerospace Laboratories, 1200 E California Blvd. MC 105-50. AIAA Fellow. E-mail: sergiop@caltech.edu

However, losing control over the deployment process, which in general is characterized by the formation and propagation of localized folds [4], is problematic. Although unconstrained deployment has been successfully demonstrated for deployable booms [5], it is too risky when deploying complex structures consisting of multiple folded shells. In such cases, the uncertainty of the deployment path of each shell would likely lead to chaotic and unpredictable behavior, potentially damaging the structure or resulting in incomplete deployment. Additional constraints exerted by a deployment mechanism can be introduced to guide the shells along a nominal deployment path.

This paper addresses the problem of controlling and predicting the constrained deployment of ultra-thin shell structures, focusing on a new type of space structure architecture, consisting of an arrangement of deployable shells that provide a planar aperture. Initially proposed in 2016 [6], this concept enables future space solar power technology by using a constellation of 60 m $\times$ 60 m independent spacecraft. The first 2 m-scale structural prototype based on this concept was developed in 2018 [7], and a deployable version of the space structure was recently demonstrated [8].

Section II provides a description of the space structure architecture and its packaging scheme. In section III, a kinematic model of the unfolding process is derived to design the nominal deployment path for the structure. Section IV introduces a computational framework that predicts the dynamic deployment behavior of the same structure, assessing the effect of the shell elasticity on the nominal kinematic path. Section V discusses the implementation of a constrained deployment scheme on a 1.7 m $\times$ 1.7 m space structure prototype, verifying the design of the deployment path and validating the kinematic and finite element models.

II. Packaging and Deployment Scheme

The space structure architecture is shown in Fig. 2. It is composed of 4 triangular quadrants, each containing several trapezoidal strips [9], connected by diagonal cords. Each strip includes 2 deployable longerons based on the triangular, rollable and collapsible (TRAC) architecture [10], connected by transverse and diagonal rods (battens), supporting functional elements for a satellite [11][12]. Two rigid joints placed on the diagonal battens connect the strips to the diagonal cords, allowing rotations about the cord axis and preventing axial displacements [13].

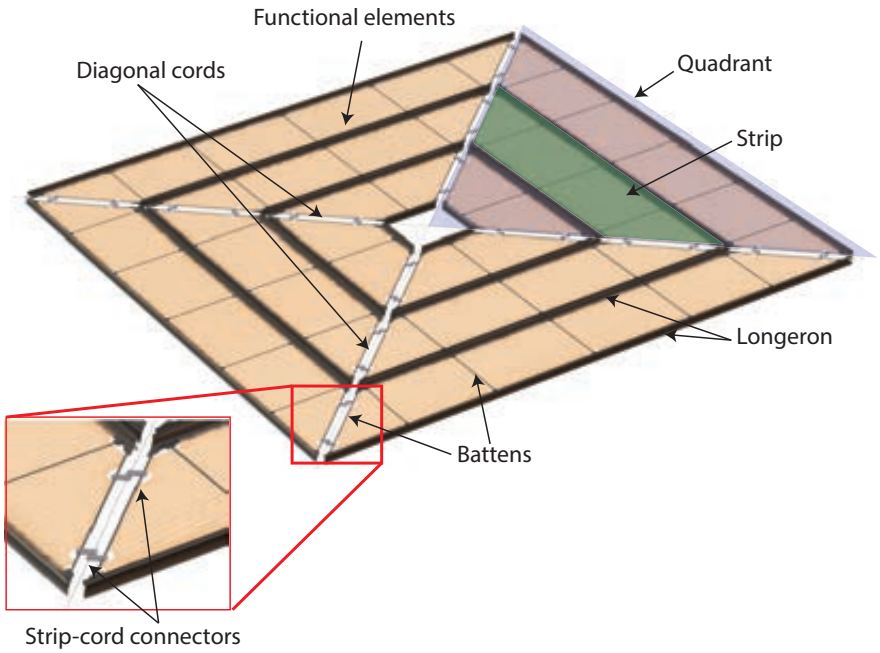

Fig. 2 Architecture of a space structure that can be packaged two-dimensionally. Each quarter of the structure contains 3 trapezoidal strips (in this example); 4 adjacent identical strips constitute a square. Each strip includes 2 longerons, connected at the ends by diagonal battens. A variable number of transverse battens connect the longerons inside the strip. The strips are supported by diagonal cords via strip-cord connectors, placed on the diagonal battens. A flexible sheet covers the interior of each strip and simulates functional elements of the spacecraft.

The structure is packaged by first z-folding each quadrant (Fig. 1, A to C) and then coiling each arm of the resulting star-shape into a cylindrical shape (Fig.1, C to E). A key aspect of this scheme is that, because of the 4-fold symmetry of the structure, z-folding the strips also requires bending the longerons. As it will be discussed later on, this aspect has important consequences on the deployment behavior of the structure.

The packaging concept described here is inspired by kirigami and was initially proposed in 2016 [6], but it was only supported by kinematic considerations and demonstrated on membrane structures. Recently, a deployment mechanism capable of actively controlling the coiling and uncoiling stage of deployment (C to E in Fig. 1) of the space structure described in this section has been successfully demonstrated [8]. However, a detailed analysis of the behavior of the real, bending-stiff structure during the unfolding stage, or possible implementations of a deployment mechanism enabling this process have not been previously considered. These are the main topics of this paper. Hence, here we will focus on the unfolding stage of the deployment (C to A in Fig. 1), aiming at achieving a predictable and repeatable behavior of the structure by guiding its deployment through external constraints.

The unfolding stage begins in the star-shape configuration, where each quadrant is z-folded and bent by 90°. Z-folding involves a low energy deformation of the structure, since adjacent strips are not physically connected along their shared edge and, therefore, are free to rotate with respect to each other. However, the strips have to bend to preserve compatibility between adjacent quadrants. The unfolding scheme considered here is based on a strain energy deployment, where the role of the external constraints is to make this process happen along a desired path.

A simple and intuitive way of guiding the deployment consists in applying clamping constraints on the strips at discrete locations and releasing the constraints sequentially, letting the structure deploy dynamically between intermediate, known configurations. In the following sections, this concept will be explored in more detail, both from a theoretical and experimental standpoint.

III. Kinematic Model

The behavior of thin shell structures subject to large rotations has been extensively studied in the past. It is well known that such structures exhibit localization phenomena, in which the cross-section of the shell locally flattens, creating regions of very low bending stiffness. Most of the bending deformation in the post-buckling regime is concentrated in these regions, known as folds.

Hence, folded shells can be modeled as essentially straight beams connected by folds, which can be approximated by elastic hinges. In the past, such models have been successfully employed to predict the quasi-static and dynamic behavior of tape springs [4][14]. In this paper, a similar approach will be used to develop a kinematic model of the strips, aimed at defining a nominal deployment path for the structure by identifying the optimal number and position of constraints. The deployment path will be described in terms of the number and position of a finite number of localized folds in each strip, throughout the unfolding process. Hence, the role of the external constraints is to impose localized folds at desired locations. When a constraint is removed, the corresponding fold is free to rotate until it latches in the deployed configuration. By sequentially removing the constraints, a sequence of intermediate equilibrium configurations can be imposed along the deployment path. However, the transition between such configurations is a dynamic process and follows a minimum energy path. Previous studies have shown that such path is not unique, since localized folds can travel along the length of the shell with constant energy [4]. Hence, the following assumptions will be used to develop a single degree-of-freedom kinematic model of a structure forming a square loop.

- The symmetry of the structure is preserved during unfolding;
- After releasing the constraints, the folds do not travel along the length of the strips;
- Longerons and battens are inextensible;
- The folds are orthogonal to the axis of the longerons;
- The battens do not deform.

The last two assumptions are justified by the relatively high bending stiffness of the diagonal and transverse battens, which makes the deformation modes in which the battens do not bend more energetically favorable. These assumptions allow us to identify a range of admissible fold locations, located within the green area of the strip in Fig. 3.

Releasable constraints connect adjacent strips in the square, so that the corresponding fold lies in a diagonal plane. When a constraint is released, the portions of the strip on the two sides of the fold rotate until they become flat. Two possible cases can be identified:

1) partial deployment, in which a constraint is removed from the strip, but other constraints are still active (Sec. III.A);
2) full deployment, in which the last constraint is removed from the strip (Sec. III.B).

In the following analysis, the evolution of the localized folds is derived as a function of an independent variable, namely the normalized deployed size, which is defined in Fig. 4.

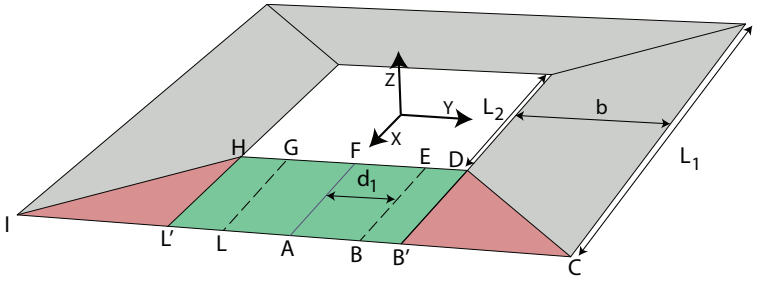

Fig. 3 Geometry of a single-square-loop structure and admissible fold locations (in green). The location of the fold EB is defined by its distance $d_1 \in \left[0, \frac{L_2}{2}\right]$ from the midplane of the strip FA. To achieve symmetric deployment, the folds EB and GL are symmetric about the midplane. When $d_1 = 0$, the two folds merge into a single fold at the center of the strip.

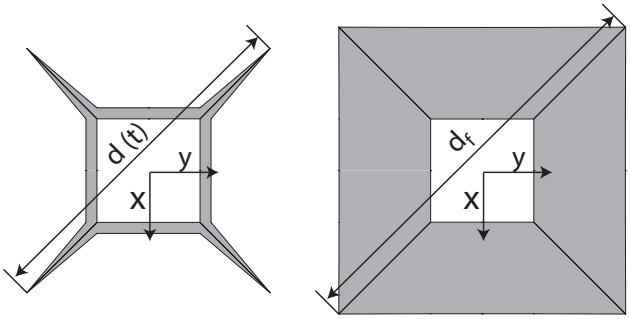

Fig. 4 Definition of normalized deployed size: $d(t)$ is the maximum diagonal size of the square loop structure, varying during the deployment; d_f is the final diagonal size. The normalized deployed size used in the kinematic analysis is defined as the ratio $\frac{d(t)}{d_f}$.

A. Partial deployment

Due to the 4-fold and mirror symmetry of the space structure architecture, it can be assumed that all strips follow the same path and remain symmetric with respect to their mid-plane. Therefore, the geometry shown in Fig. 5, containing only half of a strip, is sufficient to fully characterize the configuration of the structure.

In this model, two folds are considered, $B'E'$ and BE, respectively at a distance d_1 and d_2 from the center of the strip in the deployed state. $B'E'$ has been released, whereas the fold BE is still constrained, so it is forced to lie in the diagonal plane $P3$. Note that the same model applies to the case in which additional constraints are applied between the fold BE and the end of the strip.

To compute the evolution of the fold angles α and β during deployment, the coordinates of the 8 points $A - F$ need to be calculated. By construction, points A and F lie on the symmetry plane of the strip $P2$, defined by the equation $y = 0$ (Eq. 1a). Since the portion of the strip between AF and $B'E'$ is fully deployed, the segments AB' and FE' are normal to $P2$ (Eqs. 1b-1e).

Also, points B, C, D and E lie in the diagonal plane ($P3$), described by the equation $y - x = 0$ (Eqs. 1f-1h). To suppress rigid body motions, points A is located on plane $P1$, defined by the equation $z = 0$ (Eq. 1c). Therefore, the

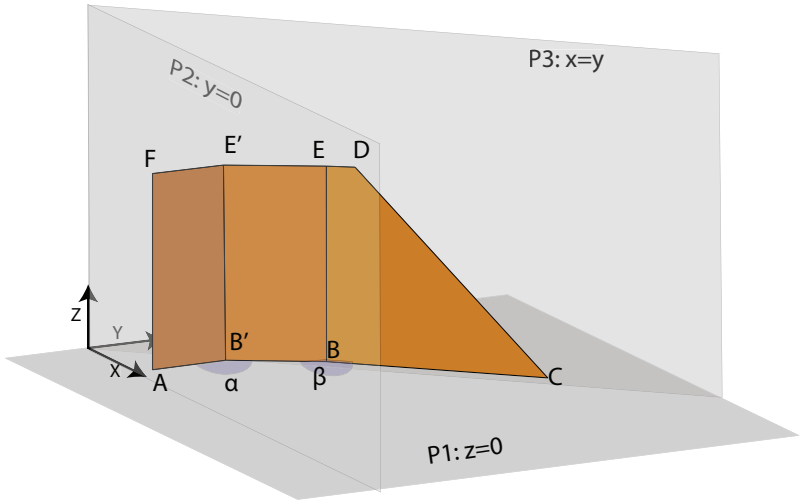

Fig. 5 One degree of freedom kinematic model for unfolding of a strip. The angles α and β describe the two folds ($B'E'$ and BE). The fold BE is constrained to stay on the diagonal plane $P3$, while $B'E'$ deploys, varying its angle from 135°to 180°.

following conditions hold:

$$y_A = y_F = 0 \tag{1a}$$
$$x_A = x_{B'} \tag{1b}$$
$$z_A = z_{B'} = 0 \tag{1c}$$
$$x_F = x_{E'} \tag{1d}$$
$$z_F = z_{E'} \tag{1e}$$
$$x_C = y_C \tag{1f}$$
$$x_D = y_D \tag{1g}$$
$$x_E = y_E \tag{1h}$$

In the star-shape configuration, the strip is orthogonal to the plane $P1$ and hence it follows that:

$$z_A = z'_B = z_B = z_C = 0 \tag{2a}$$
$$z_E = z_{E'} = z_F = b \tag{2b}$$
$$x_A = x_F \tag{2c}$$
$$x_{B'} = x_{E'} \tag{2d}$$
$$x_B = x_E \tag{2e}$$

Lastly, recalling that the fold $B'E'$ is located at a distance d_1 from the mid-plane of the strip, we write:

$$y_{B'} = y_{E'} = d_1 \tag{3}$$

Hence, the coordinates of the points A-F can be written as:

$$A = (x_A, 0, 0) \qquad F = (x_A, 0, b)$$
$$B' = (x_A, d_1, 0) \qquad E' = (x_A, d_1, b)$$
$$B = (x_B, x_B, 0) \qquad E = (x_B, x_B, b)$$
$$C = (x_C, x_C, 0) \qquad D = (x_D, x_D, b)$$

The only unknowns are x_A, x_B, x_C and x_D, subject to the following distance constraints, based on geometry and known position of the folds:

$$\|BB'\| = d_2 - d_1 \tag{4a}$$
$$\|BC\| = \frac{L_1}{2} - d_2 \tag{4b}$$
$$\|E'D\| = \frac{L_2}{2} - d_2 \tag{4c}$$

The 3 equations above, written in terms of 4 unknown variables, describe a single degree-of-freedom kinematic model, and a convenient free variable is the deployed size of the square ($d(t)$ in Fig. 3), which can be written as:

$$d(t) = 2\sqrt{2}\, x_C \tag{5}$$

Once the kinematics have been solved, the fold angles α and β, defined in Fig. 5 can be computed as follows:

$$\alpha = \frac{\pi}{2} + \arctan \frac{x_B - x_A}{x_B - d_1} \tag{6a}$$
$$\beta = \pi - \arctan \frac{x_B - x_A}{x_B - d_1} \tag{6b}$$

Note that the evolution of α and β is independent of the location of the folds, described by d_1 and d_2.

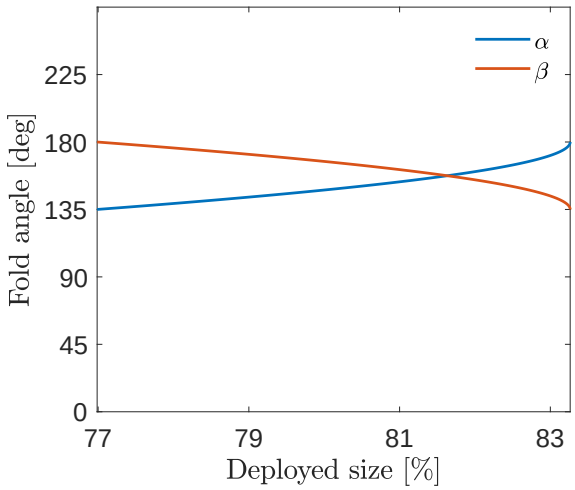

Fig. 6 Evolution of fold angles during unfolding of the inner fold ($B'E'$ in Fig. 5). The x axis corresponds to the normalized deployed size defined in Fig. 4.

B. Full deployment

Next, we consider the unfolding of a square after removing the last constraint, which activates the deployment of the fold along the dashed line BE in Fig. 7. The main difference from the previous section is that, because of the trapezoidal shape of the strip, unfolding BE also requires rotation of the strip with respect to the y axis. This results in a fully three-dimensional motion, leading to the final planar configuration.

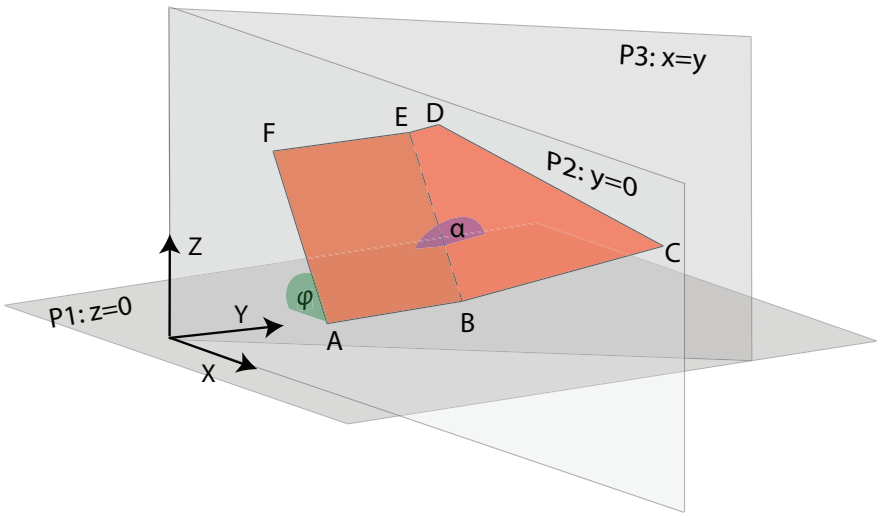

Fig. 7 One degree of freedom kinematic model of the unfolding process for a strip.

The symmetry conditions defined in Eqs. (1a),(1f) and (1g) still hold, in addition to the following:

$$x_B = x_A \tag{7a}$$
$$z_B = z_A \tag{7b}$$
$$x_E = x_F \tag{7c}$$
$$z_E = z_F \tag{7d}$$

resulting from the region $ABEF$ being already deployed. Under these assumptions, the structure has a single degree of freedom, so that it can be conveniently described in terms of the angle $\varphi \in \left[0, \frac{\pi}{2}\right]$, defined in Fig. 7. Note that $\varphi = 0$ corresponds to the fully deployed configuration and $\varphi = \frac{\pi}{2}$ to the fully folded configuration.

Geometric conditions are imposed on the length of each segment, leading to the relations:

$$x_F = x_A - b\cos\varphi \tag{8a}$$
$$y_B = y_E = d_2 \tag{8b}$$
$$z_E = b\sin\varphi \tag{8c}$$

Hence, the coordinates of the points A-F are:

$$A = (x_A, 0, 0) \qquad F = (x_A - b\cos\varphi, 0, b\sin\varphi)$$
$$B = (x_A, d_2, 0) \qquad E = (x_A - b\cos\varphi, d_2, b\sin\varphi)$$
$$C = (x_C, x_C, z_C) \qquad D = (x_D, x_D, z_D)$$

with the unknowns x_C, z_C, x_D and z_D, and the free parameter φ. To solve the kinematics, the following geometric conditions are required:

$$BE \cdot BC = 0 \tag{9a}$$
$$BE \cdot ED = 0 \tag{9b}$$
$$\|CD\| = \sqrt{2}b \tag{9c}$$
$$\|BC\| = \frac{L_1}{2} - d_2 \tag{9d}$$

where the first two equations impose orthogonality of the longerons with respect to the fold axis, whereas the remaining equations impose inextensibility of the longerons and the diagonal batten.

Using Eq. (9a):

$$(x_D - x_A)(x_c - x_D) + z_D z_C = 0 \tag{10}$$

substituting Eqs. 8 and solving for x_C, it follows that:

$$z_C = \frac{(x_C - x_A)}{\tan\varphi} \tag{11}$$

Similarly, Eq. 9b can be written as:

$$(x_F - x_A)(x_F - x_D) + z_F(z_F - z_D) = 0 \tag{12}$$

and solved for z_D, yielding:

$$z_D = z_F + \frac{x_D - x_F}{\tan\phi} \tag{13}$$

Substituting Eqs. 10 and 13 in Eqs. 9c and 9d, a system of 2 nonlinear algebraic equations in x_C and x_D is obtained, which can be easily solved numerically.

Using simple geometric relations, the fold angle α is given by:

$$\alpha = \arccos \frac{AB \cdot BC}{\|AB\| \, \|BC\|} \tag{14}$$

and is plotted in Fig. 8. As in the previous section, this plot is independent of the location of the fold EB.

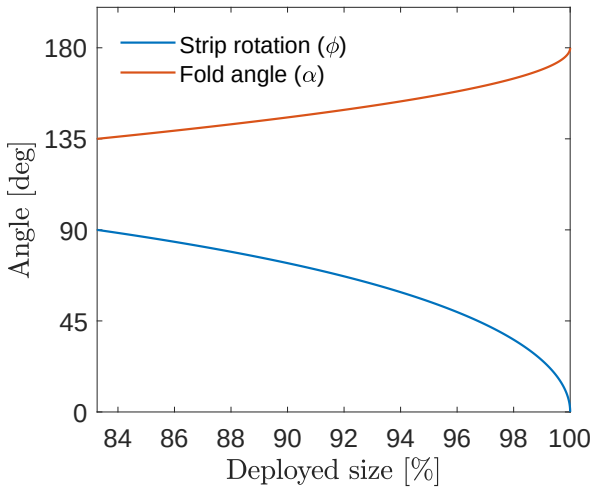

Fig. 8 Evolution of the fold angle and strip rotation angle during the final step of the strip deployment. The x axis corresponds to the normalized deployed size defined in Fig. 4.

C. Unfolding kinematics of a full module

The kinematic analysis presented so far can be extended to model the deployment path of an entire module, consisting of multiple square loops, by adding suitable compatibility conditions. Such conditions are required to prevent penetration between different strips in the same quadrant and to account for the presence of cords of fixed length connecting them.

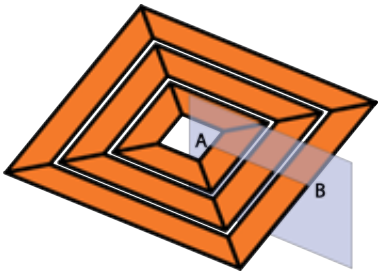

(a) Section plane on a 3 square space structure

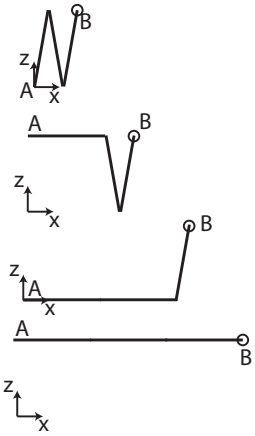

(b) Section view of a 3-step deployment scheme, in which one square at a time is released.

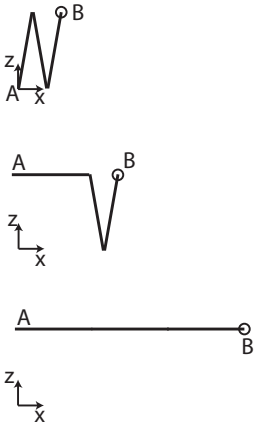

(c) Section view of a 2-step deployment scheme, in which the innermost square is released first, followed by the middle and outer squares released simultaneously.

Fig. 9 Comparison between 2-step and 3-step release schemes. The outer edge (point B) is assumed to be at a fixed height (z coordinate). When releasing one square at a time, point A is forced to move in the vertical direction during unfolding of the other strips; when releasing 2 squares simultaneously, point A remains fixed after unfolding of the inner strip.

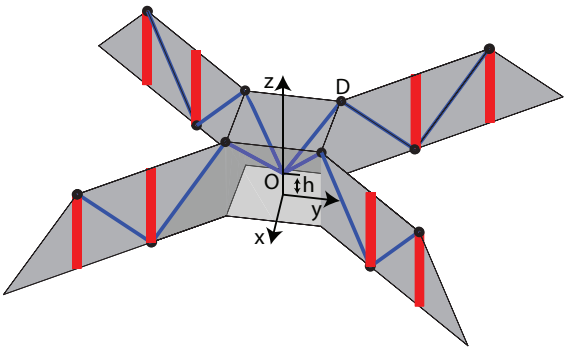

(a) 3-square loop structure with diagonal cords (blue lines). The cords are connected to point O, fixed on the central axis. h is the distance of this point from the horizontal plane $z = 0$.

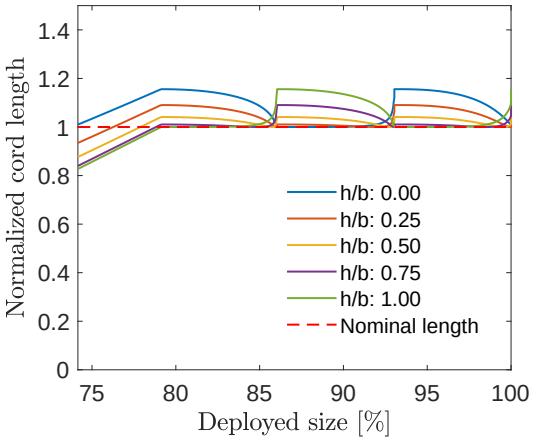

(b) Distance OD normalized by its final value, as a function of the normalized deployed size (Fig. 4). Different lines correspond to different locations of point O on the z axis. The dashed red line corresponds to the length of the cord required at the end of the deployment.

Fig. 10 Distance between the innermost strip and the central axis during a 3-step unfolding scheme.

In this section, an optimal deployment path for a planar structure consisting of multiple square loops is developed, by choosing the number and position of localized constraints. When choosing the number of constraints, an intuitive solution would be to introduce as many constraints as the number of squares in the structure, in order to deploy one square at a time. Additional constraints would only add intermediate partial deployment steps, at the cost of increased complexity of the system. On the other hand, reducing the number of constraints would simplify the release mechanism, but it would require simultaneous unfolding of multiple squares at the same time.

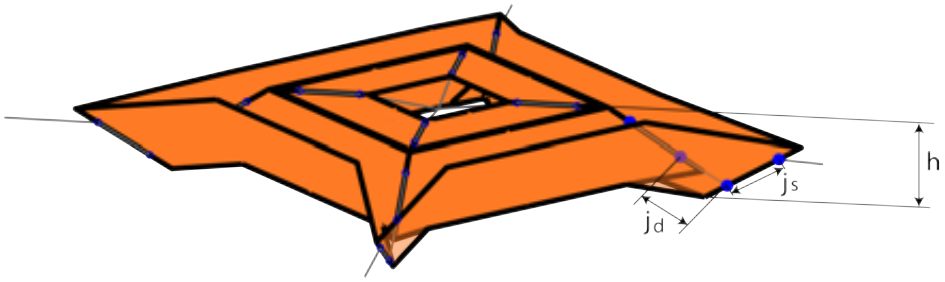

(a) Geometry of a 3 square loop structure during unfolding. Blue circles represent the strip-cord connectors. j_s is the joint spacing, whereas j_d is the distance between joints on adjacent strips. h is the maximum strip height, which can be greater than the strip width b due to the out-of-plane motion of the strips during unfolding.

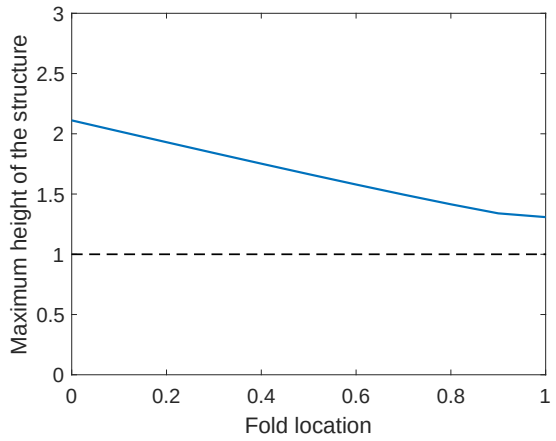

(b) Maximum height h of a 3 square loop structure during unfolding, as a function of the fold location. Height h is normalized by the strip width b (dashed line); fold location is normalized so that 0 corresponds to the center of the strip and 1 to the tip of the shortest longeron of the strip.

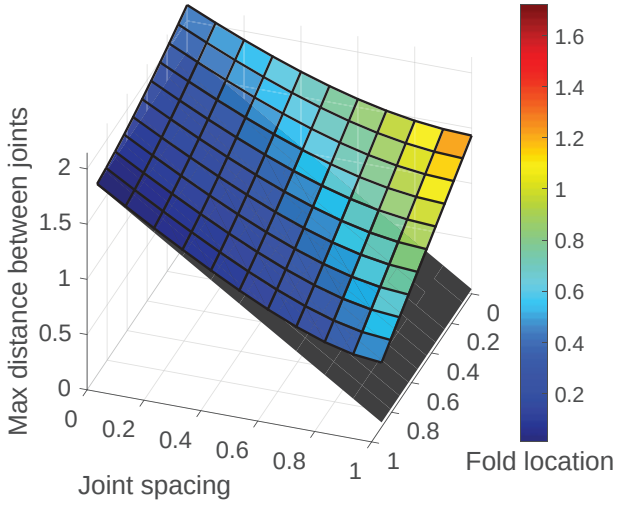

(c) Maximum distance j_d between strip-cord connectors of adjacent strips in a 3 square loop structure. The grey surface corresponds to their distance in the deployed state (equal to length of the cords). The color map corresponds to the difference between maximum joint distance j_d and cord length, normalized by the strip width b. Fold location is normalized so that 0 corresponds to the center of the strip and 1 to the tip of the shortest longeron; joint spacing j_s is normalized by its maximum value.

Fig. 11 Effect of fold location on kinematics and boundary conditions. b) shows that, by moving the fold towards the center of the strip, the maximum height of the structure during unfolding increases. c) shows that moving the fold towards the center of the strip increases the maximum distance between strip-cord connectors of adjacent strips, resulting in incompatible kinematics. Increasing the joint spacing on the strips has a similar effect, although much less pronounced.

Particularly interesting is the case of deploying 2 squares at a time, shown in Fig. 9 for a 3 square loop structure. In the intuitive approach of releasing one square at a time (Fig. 9b), the innermost point of the structure (A) is forced to move along the vertical axis during unfolding of the other strips. In the concept of releasing 2 squares at a time (Fig. 9c), point A remains fixed after unfolding the innermost strip. This has important implications from a practical perspective, since some implementations of the space structure discussed in this work require the diagonal cords to be attached to a fixed point on the central axis of the structure. As it will be discussed in more detail in Sec.V, this allows to tension the cords at the end of the deployment, which is necessary to exploit the full potential of the structure from

the structural dynamics standpoint. Specifically, previous studies [9] have shown the existence of a threshold on the cord pre-stress, corresponding to the transition from cord-dominated to strip-dominated vibration modes.

Fig. 10 tracks the distance of the innermost point (D) of a 3 square loop structure from a fixed point O on the central axis during a 3-step unfolding process. Each line corresponds to a different height of point O. The plot shows that, regardless of the location of the attachment point, releasing one square at a time would lead to incompatible boundary conditions, since the maximum distance OD always exceeds the length of the cord. As a consequence, buckling of the structure and incomplete deployment would likely occur if such unfolding scheme was implemented.

By releasing two squares simultaneously, the height of point D would not change after unfolding the first strip. In this case, Fig. 10b shows that, for $h/b = 1$ (i.e. the cord is attached at the top of the folded structure), the distance OD increases monotonically during unfolding of the first square and reaches its maximum value at the nominal length of the cord. After this point, the distance OD remains constant during deployment of the remaining squares. Therefore, a fixed center point unfolding requires at least 2 squares being released at the same time. For a 3 square loop structure, this results in a 2-step unfolding process, in which the inner strip is released first, followed by the remaining two strips deploying simultaneously. These conclusions can be extended to larger structures, for which admissible unfolding schemes require simultaneous deployment of an even number ($2m$) of squares, with the exception of the innermost n squares. Here, n and m are positive integer numbers, and their choice results from a trade-off between controlling the deployment process and minimizing the number of releasable constraints.

Next, we consider the effect of the fold location, defined in Fig. 3: as shown in Fig. 7, deployment requires opening of the fold angle α and rotation of the strip from the horizontal plane (described by the angle φ). As a result of this motion, the tip of the strip (C) moves in the out-of-plane direction. It can be shown that the magnitude of this displacement depends on the fold location, increasing as the fold moves towards the center of the strip. This has two practical implications: first, it affects the maximum height of the structure during unfolding; second, it affects the maximum distance between the tips of adjacent strips in a quadrant.

Fig. 11a examines the effect of the fold location on the maximum height of the structure during unfolding. The analytical model shows that, by moving the fold towards the center of the strip, the maximum height of the structure becomes more than double its value in the folded state. This implies that significant clearance would need to be provided in order to avoid interferences with the deployment mechanism containing the space structure.

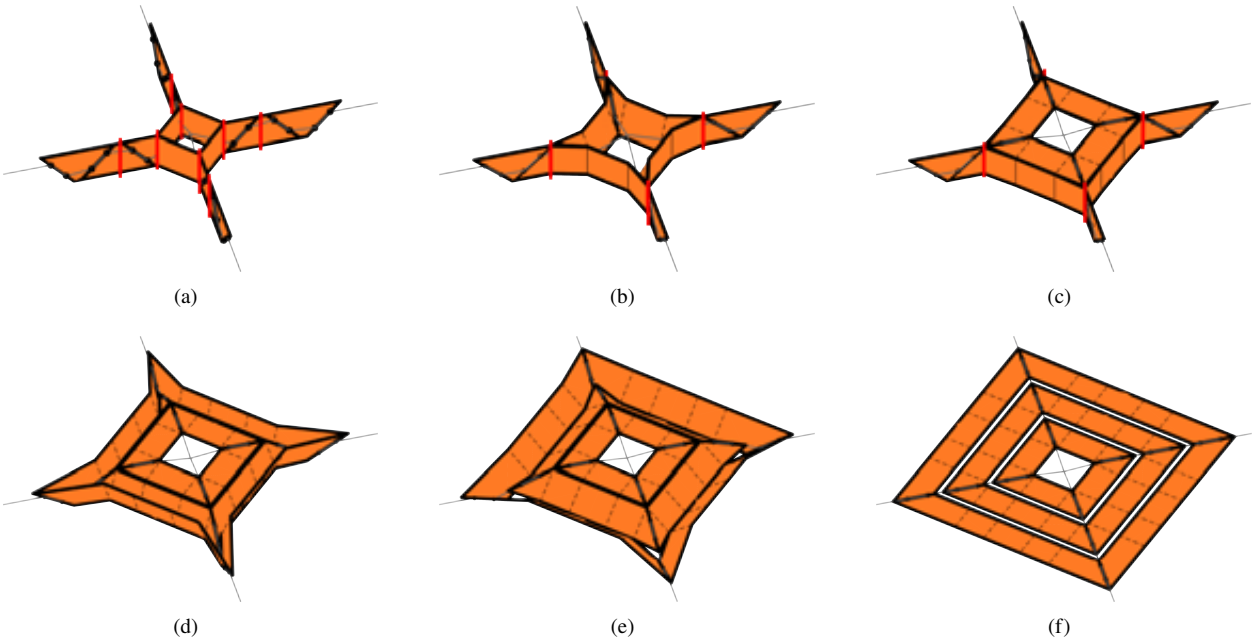

Fig. 12 Deployment sequence from kinematic model for a 2-step deployment scheme with fixed folds. The red lines represent the localized constraints, which are simultaneously removed on the 4 arms of the star-shape. Dashed lines correspond to fixed localized folds. (a) to (c) shows the release of the first set of constraints, resulting in the deployment of the inner square. (d) to (f) shows the deployment of the middle and outer squares, following the release of the second set of constraints.

Fig, 11b investigates the effect of the kinematic path on the boundary conditions between strips, specifically focusing on the diagonal cords connecting adjacent strips in a quadrant. The figure shows that the maximum distance between joints of adjacent strips depends on the fold location and the spacing between joints in the same strip. If their maximum distance is greater than the length of the cord (shown in grey), interference will occur during unfolding. The color map in the surface plot corresponds to the difference between maximum distance and cord length, which should be zero in the ideal case. It can be observed that their difference increases as the fold location moves toward the center of the strip and the joint spacing increases. Based on these considerations, the analytical model suggests that the localized constraints should be placed as far as possible from the center of the strips, while avoiding bending of the diagonal battens.

Fig. 12 shows the nominal deployment sequence for a 3 loop square structure. The red lines correspond to the locations of the active constraints, which are sequentially released in a 2-step process, starting from the innermost ones.

IV. Numerical Model of Deployment

The analytical model presented so far has provided a sequentially controlled deployment scheme for the space structure described in Sec. II. However, this model was only based on kinematics and did not take into account the mechanical response of the structure and how this impacts the formation and evolution of the localized folds during deployment. In this section, a finite element model of the deployment process of the space structure will be developed, using the commercial software Simulia Abaqus 2018.

First, a single square loop structure is considered. Then, the model is extended to a three square loop structure and results for a 1.7 m $\times$ 1.7 m structure are presented.

A. Single square loop

The smallest unit structure for which the deployment can be tested is a single square loop. In the ideal case, the following conditions hold:

1) The 4-fold symmetry of the structure is preserved during deployment;
2) The mirror symmetry of each strip is preserved during deployment.

The first assumption allows to model a single strip as representative of the entire square, by exploiting the symmetry of the structure. However, the deployment path of each strip may not be symmetric. The second assumption enforces the highest degree of symmetry, allowing to model only half of a strip as representative of the entire square. Although a real structure might also exhibit symmetry-breaking deployment paths, the assumptions listed above focus on the nominal deployment path of the structure.

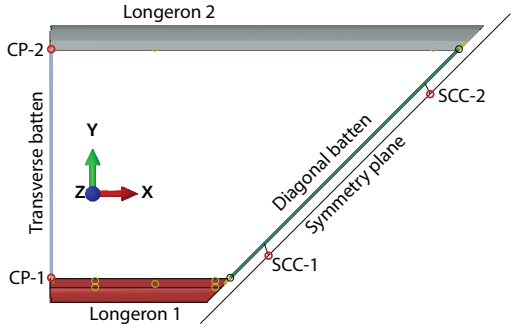

Fig. 13 Symmetric model of a single-square structure. SCC-1 and SSC-2 are the strip-cord connectors; CP-1 and CP-2 are the control points at each end of the transverse batten.

The resulting model is shown in Fig. 13: the longerons are modeled with S4R reduced-integration shell elements, whereas the battens are represented by B13 linear 3D beam elements, with rectangular cross-section. The geometry of longerons and battens represents the structural prototypes described in previous work [7][8]. Each flange of the longerons is orthotropic and consists of a [±45GF/0CF/±45GF] laminate, as described in [15].

The two halves of the longerons are bonded along their web by tie constraints, and the battens are connected to the longerons by using kinematic coupling constraints between the end node of the batten and a 2 mm $\times$ 2 mm region of influence on the longerons. The strip-cord connectors are modeled as reference points (SSC-1 an SSC-2 in Fig. 13) connected to the diagonal batten by kinematic couplings.

Based on the assumptions discussed previously, symmetry is enforced by the following boundary conditions:

- X-symmetry is defined at the left end of both longerons;
- A discrete rigid plane, oriented along the diagonal direction, keeps the strip within its symmetry domain through contacts;
- The linear constraint equation $u_x = u_y$ is imposed to the strip-cord connectors (SSC-1 and SSC-2), to keep them on the diagonal plane and enforce continuity between strips.

The analysis consists of 3 phases: folding, equilibrium and deployment. In the first step, the structure is quasi-statically z-folded from its deployed state into a star-shape. In the second step, localized constraints are applied and any residual kinetic energy in the model is dissipated, providing the final folded configuration. Finally, the constraints are suddenly removed and the structure is let dynamically deploy by releasing its strain energy.

To guide the folding process, two control points are defined (CP-1 and CP-2 in Fig. 13), coinciding with the end nodes of the transverse batten. Displacement boundary conditions are applied to these points to mimic the folding procedure developed for the physical prototype of the space structure. Specifically, the conditions are:

- $u_z = 0,\ u_y = 0$ at CP-1;
- $u_z = b$ at CP-2, where b is the width of the strip.

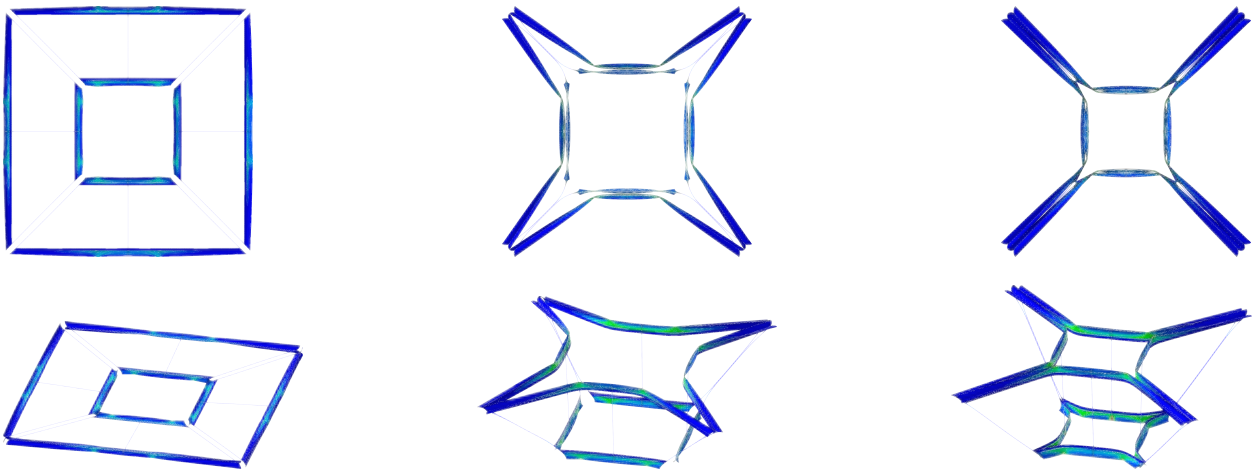

Fig. 14 Folding simulation of a single-square loop structure.

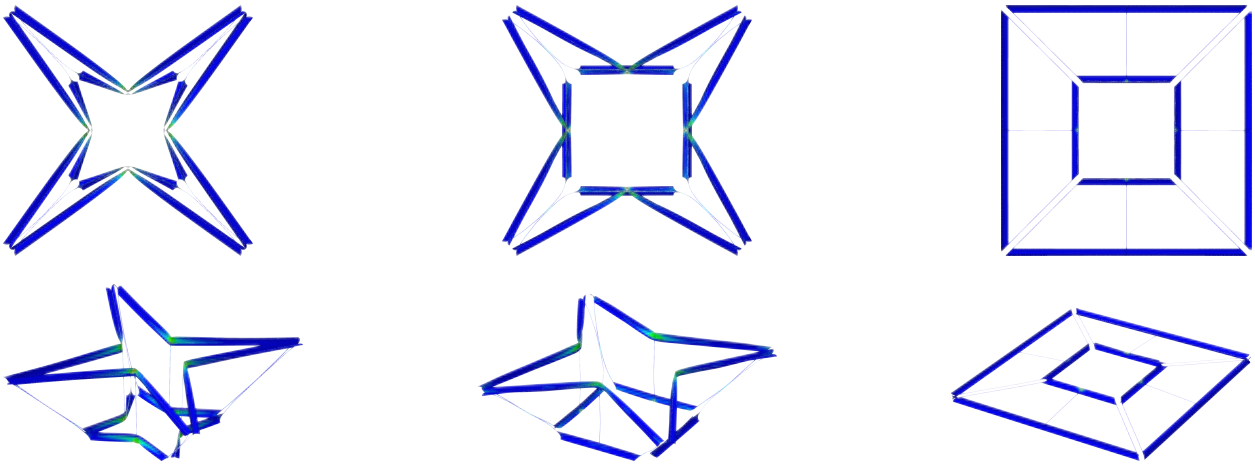

Fig. 15 Deployment simulation of a single-square loop structure.

This suppresses rigid body motions in the out-of-plane direction, while forcing the outer longeron to rotate about the inner one, folding during this process. Auxiliary localized folds are created at specific locations of the longerons to

get to the star-shape, by applying pressure on both flanges. The constraints connecting adjacent strips are modeled by pressure loads on a narrow strip of elements on the longerons, pushing them against the diagonal plane. Contacts are modeled using a frictionless hard contact definition, enforced by a penalty method.

Two solution approaches were considered: implicit dynamics and explicit dynamics. The advantage of the former is to be unconditionally stable, allowing it to use relatively large time increments during the quasi-static folding step. Also, the implicit solution tends to be less noisy and more accurate than the explicit one. On the other hand, an explicit scheme is more suited for large problems with severe nonlinearities (i.e. instabilities and complex contact conditions) and is commonly used for deployment problems [16].

For the problem at hand, preliminary deployment simulations had shown that the stability of the implicit solver rapidly degrades when multiple shells interact in complex contact conditions, thus making it necessary to use an explicit dynamics solution.

Fig. 14 shows the results of the folding process for a one-square structure. The full square is shown for visualization purposes, although only 1/8 of it was actually modeled (as described previously in this section). The results from free deployment are shown in Fig. 15.

It can be observed that, upon release of the four constraints, the folds propagate towards the center of the strips and merge before deploying. Also, the shorter longeron deploys before the other one, due to the smaller inertia.

B. 3 square loops

In this section, a finite element model of a 3 square space structure is developed. Symmetry is applied to model only 1/8 of the structure, as shown in Fig. 16. Each strip is modeled as described in the previous section. Adjacent strips are connected by cords, modeled as connector elements between the strip-cord connectors. The cords impose an upper bound to the distance between the strip-cord connectors, but they do not constrain the minimum distance, since the cords cannot bear any load in compression.

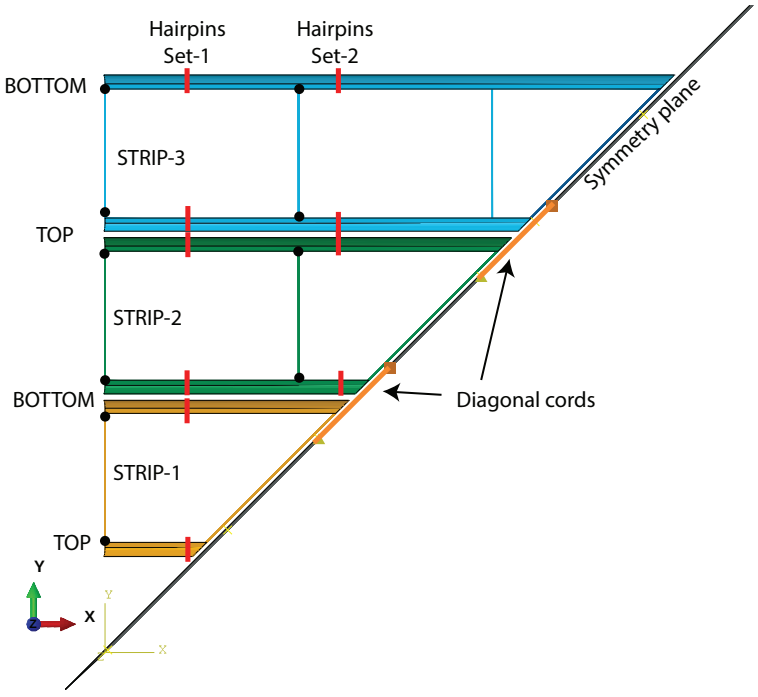

Fig. 16 Finite element model of a 1.7 m × 1.7 m 3-square loop structure. The model assumes 4-fold symmetry and mirror symmetry, thus allowing to consider only 1/8 of the whole structure. The location of the localized constraints is indicated by the red lines. During deployment, Hairpin Set-1 is released first, followed by Hairpin Set-2. The strip-cord connectors are modeled as reference points moving on the symmetry plane. Adjacent strips are connected by cords, modeled as axial connectors with one-sided hard stop behavior.

The red lines in Fig. 16 correspond to the locations of the localized constraints. Also, the labels top and bottom

indicate mountain and valleys folds during star folding.

The analysis consisted of the following steps:

1) Z-fold: vertical displacements $u_z = b$ are assigned to the control points on the mountain folds, while the valley folds are fixed. Localized folds are created at designated locations by applying pressure on narrow regions of the longerons.
2) Tighten: radial displacements are applied to the outermost strip to tighten the structure into a star shape (Fig. 17(b)-17(c)).
3) Apply constraints: "hairpins" are applied to the structure by using pressure at the locations shown in Fig. 16, pushing the longerons against the diagonal plane (Fig. 17(d)).
4) Stop: viscous pressure is introduced to dissipate the residual kinetic energy and reach a stationary fully folded configuration.
5) Release inner constraints: pressure is removed from the first set of constraints to allow deployment of the inner square (Fig. 17(e)).
6) Release outer constraints: pressure is removed from the second set of constraints to allow full deployment of the structure (Fig. 17(f)).

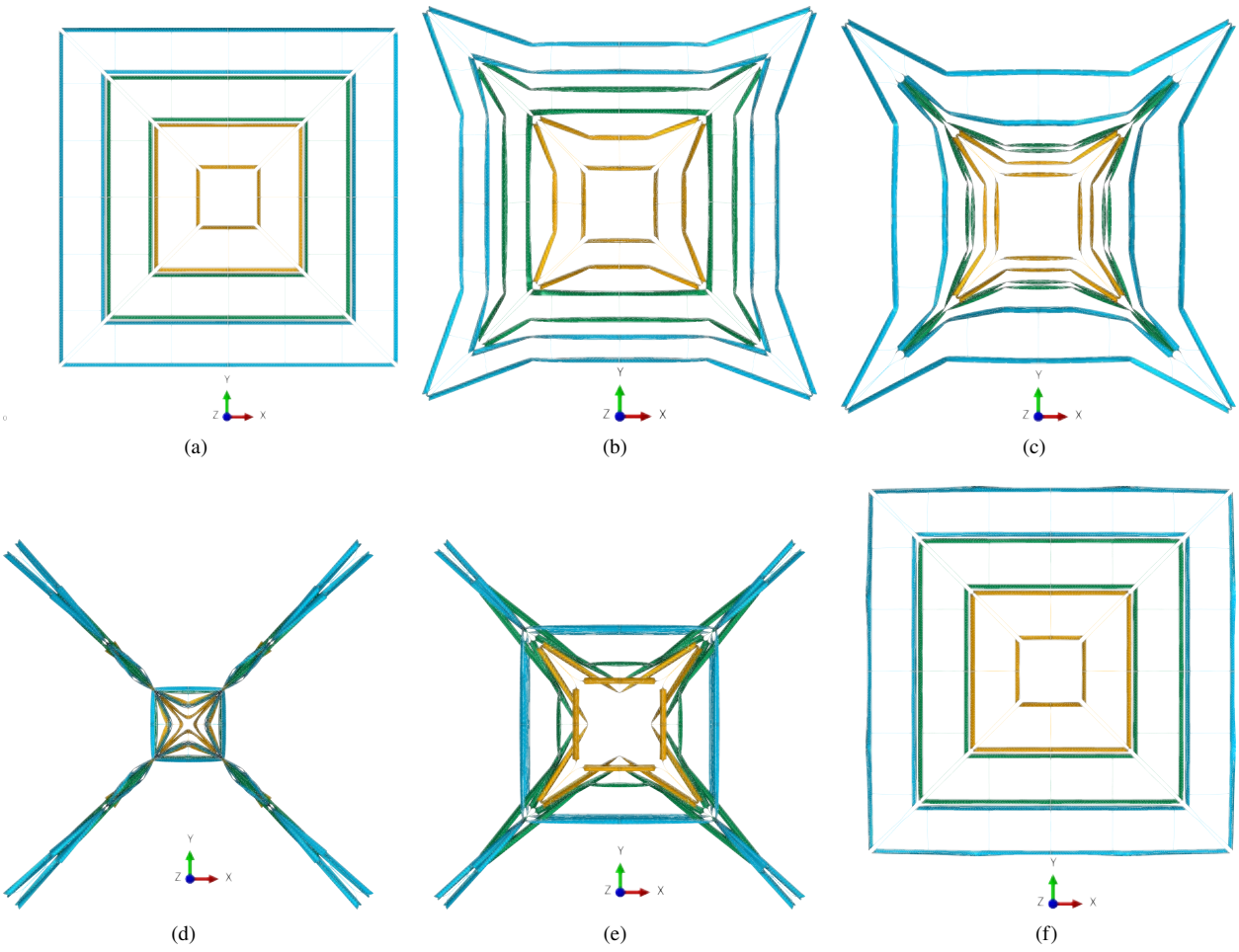

Fig. 17 Deployment simulation of a 3-square loop structure. a) to c) describe the folding process; d) is the fully folded configuration; e) is the intermediate configuration after releasing the first constraint; f) is the final configuration after releasing the second constraint.

The simulation shows that, after releasing the first set of constraints, the inner square (yellow in Fig. 17) does not reach the fully deployed state as predicted by the kinematic model. The reason is that there is insufficient space for the inner square to deploy, caused by the width of the flanges of the undeployed squares. However, after releasing the

second set of constraints, the inner square completes its deployment, followed by the middle square (green in Fig. 16) and finally by the outer square (blue in Fig. 16).

V. Deployment Experiments

The unfolding scheme developed in the previous sections was demonstrated on a deployable 1.7 m $\times$ 1.7 m space structure prototype [8].

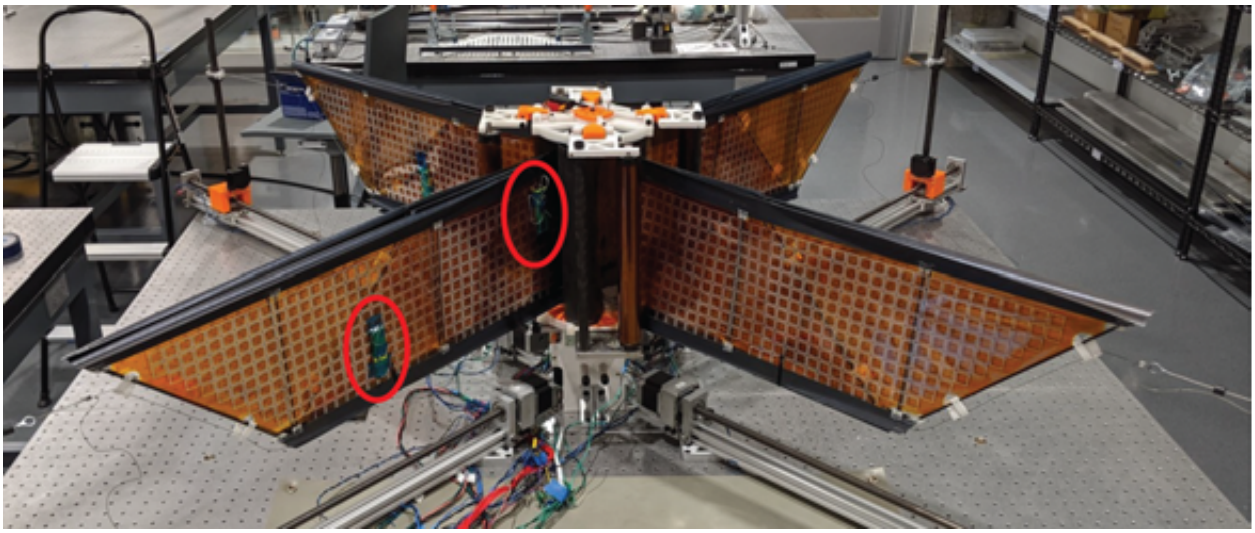

Fig. 18 Experimental setup for the deployment tests. The red circles show the locations of the localized constraints.

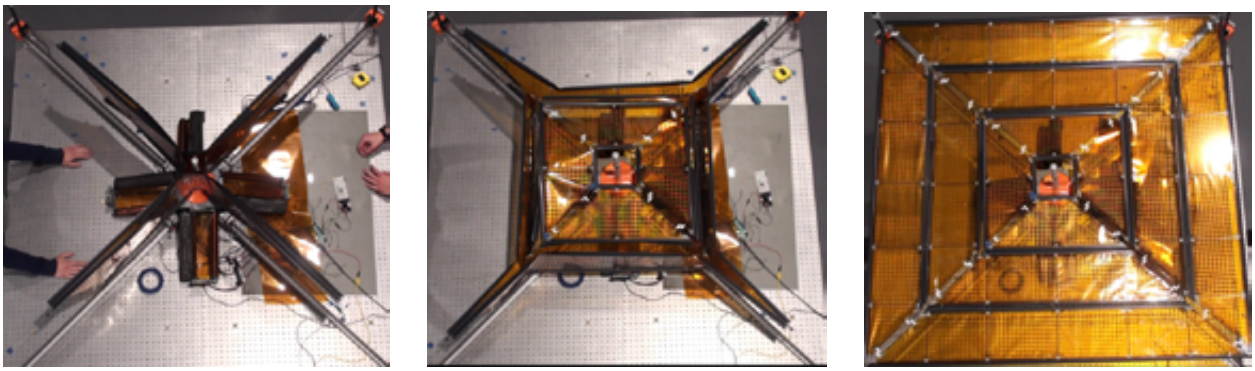

(a) Initial (b) Deployment of inner square (c) Deployment of middle and outer squares

Fig. 19 Test 20: intermediate configurations of 2-step sequential dynamic deployment.

To obtain the packaged configuration required for the unfolding, the structure was manually folded and constrained at discrete locations by using hairpins. The folded structure was mounted in a deployment mechanism by attaching the inner end of the diagonal cords to a central shaft. The deployment mechanism, which controls coiling and uncoiling of the structure, was only meant to provide support to the structure during the unfolding tests and will not be discussed further in this paper (more details are provided in [8]). The outer end of the diagonal cords of the space structure were connected to a cord management system, consisting of a spring retractor that applied a small amount of tension (less than 4 N) during and after the unfolding process.

A two-step unfolding process was attempted, with the localized constraints initially placed at the optimal location identified by the kinematic model. As a proof of concept of the deployment scheme, the constraints were applied by

hairpins that were removed manually. Future implementations of the concept will include a remotely controlled release system.

Initial experiments identified interferences between adjacent longerons of strips in the same quadrant, at the end of the first release stage, similarly to what had been predicted by the finite element model (Fig. 17(e)). As anticipated in Sec. IV, the cause of the interference was related to the finite width of the shells, which had not been taken into account in the analytical model, and resulted in a reduction of the available space for the inner square to deploy. Consequently, contact between adjacent longerons resulted in incomplete deployment of the inner square in the intermediate configuration. To address this issue, the location of the hairpins was modified to increase the inner spacing at the end of the first deployment step. However, this solution was not kinematically compatible with the model described in the previous section (it required a fold in the non-admissible region of Fig. 3) because it involved bending of the diagonal battens. In practice, the 600 μm-thick battens were flexible enough to allow such kinematics, but the resulting bending moments applied on the longerons could cause buckling of the strips. Therefore, an iterative approach was used to optimize the location of the second set of constraints such that the inner square could fully deploy after releasing the first set of constraints.

Fig. 19 shows the intermediate configurations of the modified deployment path, which resulted in a predictable and symmetric process.

VI. Discussion

It has been shown that, by adding releasable constraints, predictable and controlled deployment of a complex planar shell structure can be achieved. By identifying kinematic paths compatible with the boundary conditions and geometry of the structure, a kinematic analytical model provides a simple tool to design a sequential deployment scheme. The model suggests that releasing two squares at a time prevents interferences when the structure is supported by taut cords. Also, placing the constraints as close as possible to the ends of the strips minimizes the deployment envelope (and size of the deployment mechanism) and mitigates interference with the cords connecting adjacent strips.

The finite element model confirmed that the kinematic design actually leads to full deployment of the structure. It also captured the actual behavior of the elastic folds, which tend to propagate and merge during deployment, if their initial distance is sufficiently small (e.g. on the inner set of localized folds). Furthermore, the finite element model was successful at predicting incomplete deployment of the inner strips after releasing the first set of constraints, due to contacts between strips. Although additional work is required to improve the numerical model, the results so far suggest that it can provide a high fidelity representation of the actual deployment, and identify potential incompatibilities not captured by a simple kinematic analysis.

The experimental results show that, after improving the location of the constraints, the desired intermediate configurations could be achieved during unfolding of a space structure prototype. Future work will focus on collecting quantitative measurements of the deployment process, in order to capture the evolution of the structure during dynamic deployment and compare the dynamic response with the prediction from the finite element model.

VII. Conclusion

We have presented a novel approach to the design and control of the deployment of folded thin-shell structures, taking as an example a planar structural architecture developed for space solar power applications. We showed that releasable external constraints can efficiently control the deployment path of a strain-energy-deployed structure, by imposing known intermediate configurations.

We showed that, by treating the localized folds as hinges between rigid portions of the shells, the actual continuous structure can be modeled as a finite degree-of-freedom mechanism. The analytical model derived in this work provided a powerful tool to quickly explore the design space of a sequentially controlled deployment scheme, identifying kinematically-compatible deployment paths and an initial design point for the localized constraints. A numerical framework was developed to provide an high fidelity model of the structure, capturing its elastic response and its interaction with the constraints.

By extending the methods discussed so far to more general structural architectures, this work can contribute to the design of a new generation of large deployable structures for space applications, allowing folding and coiling techniques to be combined to achieve robust and repeatable deployment.

Acknowledgments

The authors acknowledge financial support from the Space Solar Power Project at Caltech. Prototype component fabrication and assembly support from Mr. Alan Truong is gratefully acknowledged.

References

[1] Straubel, M., Seefeldt, P., Spietz, P., and Huehne, C., "The design and test of the Gossamer-1 boom deployment mechanisms engineering model," *2nd AIAA Spacecraft Structures Conference*, 2015, p. 1837.

[2] Spence, B. R., White, S., LaPointe, M., Kiefer, S., LaCorte, P., Banik, J., Chapman, D., and Merrill, J., "International Space Station (ISS) Roll-Out Solar Array (ROSA) Spaceflight Experiment Mission and Results," *2018 IEEE 7th World Conference on Photovoltaic Energy Conversion (WCPEC)(A Joint Conference of 45th IEEE PVSC, 28th PVSEC & 34th EU PVSEC)*, IEEE, 2018, pp. 3522–3529.

[3] Marks, G. W., Reilly, M. T., and Huff, R. L., "The lightweight deployable antenna for the MARSIS experiment on the Mars express spacecraft," *36th Aerospace Mechanisms Symp*, 2002, pp. 183–196.

[4] Seffen, K., and Pellegrino, S., "Deployment dynamics of tape springs," *Proceedings of the Royal Society of London. Series A: Mathematical, Physical and Engineering Sciences*, Vol. 455, No. 1983, 1999, pp. 1003–1048.

[5] Mobrem, M., and Adams, D., "Deployment analysis of the lenticular jointed antennas onboard the mars express spacecraft," *Journal of Spacecraft and Rockets*, Vol. 46, No. 2, 2009, pp. 394–402.

[6] Arya, M., Lee, N., and Pellegrino, S., "Ultralight structures for space solar power satellites," *3rd AIAA Spacecraft Structures Conference*, 2016, p. 1950.

[7] Gdoutos, E., Leclerc, C., Royer, F., Türk, D. A., and Pellegrino, S., "Ultralight spacecraft structure prototype," *AIAA SciTech Forum*, 2019, p. 1749.

[8] Gdoutos, E., Truong, A., Pedivellano, A., Royer, F., and Pellegrino, S., "Ultralight Deployable Space Structure Prototype," *AIAA SciTech 2020 Forum*, 2020.

[9] Royer, F., and Pellegrino, S., "Ultralight ladder-type coilable space structures," *AIAA SciTech Forum*, 2018, p. 1200.

[10] Murphey, T. W., and Banik, J., "Triangular rollable and collapsible boom," , Mar. 1 2011. US Patent 7,895,795.

[11] Gdoutos, E., Leclerc, C., Royer, F., Kelzenberg, M. D., Warmann, E. C., Espinet-Gonzalez, P., Vaidya, N., Bohn, F., Abiri, B., Hashemi, M. R., et al., "A lightweight tile structure integrating photovoltaic conversion and RF power transfer for space solar power applications," *AIAA SciTech Forum*, 2018, p. 2202.

[12] Hashemi, M. R. M., Fikes, A. C., Gal-Katziri, M., Abiri, B., Bohn, F., Safaripour, A., Kelzenberg, M. D., Warmann, E. L., Espinet, P., Vaidya, N., et al., "A flexible phased array system with low areal mass density," *Nature Electronics*, Vol. 2, No. 5, 2019, p. 195.

[13] Türk, D. A., and Pellegrino, S., "Parametric Design of Conforming Joints for Thin-Shell Coilable Structures," *AIAA SciTech Forum*, 2019, p. 1259.

[14] Hohmann, B., Sakamoto, H., and Okuma, M., "Influence of Storage Configurations on the Deployment Behavior of Boom-Membrane Integrated Space Structures," *AIAA SciTech Forum*, 2019, p. 1016.

[15] Leclerc, C., and Pellegrino, S., "Reducing Stress Concentration in the Transition Region of Coilable Ultra-Thin-Shell Booms," *AIAA SciTech Forum*, 2019. doi:10.2514/6.2019-1522, URL `https://arc.aiaa.org/doi/abs/10.2514/6.2019-1522`.

[16] Mallikarachchi, H., and Pellegrino, S., "Quasi-static folding and deployment of ultrathin composite tape-spring hinges," *Journal of Spacecraft and Rockets*, Vol. 48, No. 1, 2011, pp. 187–198.